Efficiency of Background Suppression for Arterial Spin Labeling

by

Dairon Garcia

Submitted to the Department of Electrical Engineering and Computer Science
in partial fulfillment of the requirements for the degree of

Masters of Engineering in Electrical Science and Engineering

at the

MASSACHUSETTS INSTITUTE OF TECHNOLOGY

May 2004

Author .....
Department of Electrical Engineering and Computer Science
May 18, 2004

Certified by ...
David Alsop
Associate Professor of HST
Thesis Supervisor

Accepted by .....
Arthur C. Smith
Chairman, Department Committee on Graduate Students

The Efficiency of Background Suppression in Arterial Spin Labelling

by

Dairon Garcia

Submitted to the Department of Electrical Engineering and Computer Science
on May 18, 2004, in partial fulfillment of the
requirements for the degree of
Masters of Engineering in Electrical Science and Engineering

Abstract

Arterial spin labeling (ASL), a technique developed for the measurement of local tissue perfusion with MRI, is heavily dependent on distinguishing irrelevant static tissue signal from the labeled blood. Background suppression can greatly reduce motion and other sources of noise in Arterial Spin Labeling MRI. More sophisticated background suppression strategies with many inversion pulses may decrease the ASL signal causing reduced signal-to-noise ratios and quantitative accuracy. Numerical simulations and in-vivo measurements were used to measure the inefficiency of different adiabatic inversion pulses and to optimize pulse selection. The results emphasize the high potential efficiency of adiabatic inversion pulses but also the limited optimal range of pulse parameters.

Thesis Supervisor: David Alsop
Title: Associate Professor of HST

Contents

List of Figures

List of Tables

Chapter 1

Introduction and Theory

This section attempts to summarize the basic components of Magnetic Resonance Imaging that were necessary to understand throughout the course of this study. Although these concepts are extremely condensed here, there is sufficient detail for reproducibility without much prior external instruction in the field.

1.1 Motivation for MRI and basic MRI physics

As of yet, it is still impossible to witness, account for, and accurately measure individual action potentials while the brain is being activated. Even invasive methods of determining electrical activity in certain areas of the brain can be confounded by various remote and local electrical factors that are also not well understood. Determining electric potentials and magnetic field differences in different areas of the brain can be confounded in similar ways and often provide either too remote or too non-specific (or "averaged") a measurement to be correlated precisely enough to action potentials. However, observable local hemodynamic changes that are coupled with activation help determine particular tissue functions without probing the brain with electrodes or exercising other invasive or imprecise procedures. Functional Magnetic Resonance Imaging (fMRI) provides a noninvasive means of making these observations. It makes use of the properties of magnetic moments produced by individual hydrogen nuclei when placed in a magnetic field. Hydrogen molecules are of interest

because blood is composed of mostly water, and hydrogen atoms are mostly found in water and fat. Magnetic moment vectors are observed when nuclei with unequal number of protons and neutrons experience a static magnetic field [2].

Each subatomic particle possesses a fundamental property of "spin" (or angular momentum) and charge. A moving electrical charge possesses a magnetic field. This is because spin can be thought of as equivalent to a circulating electric current, which creates a magnetic field. A proton's magnetic field is a point dipole, which can be thought of as an individual magnetic moment vector that aligns itself parallel (low energy spin state) or antiparallel (high energy state) to an applied external magnetic field at equilibrium. The composite nuclear magnetic vector, or net vector of spins experiencing approximately the same magnetic field strength, also aligns itself similarly to the magnetic field. When not aligned with the axis, the vector also rotates about the axis at a frequency:

$$\omega_0 = \gamma B_0 \tag{1.1}$$

where ω_0 is called the larmor or resonance frequency, γ is the observed gyromagetic ratio or spin frequency per magnetic field strength (depends on size and shape of nucleus), and B_0 is the applied magnetic field achieved by passing a current through a large coil (magnet) [8]. When a nuclear spin system is exposed to energy applied at the larmor frequency (when ω equals ω_0), the magnetic moments flip between the two energy spin states. The equation below gives the relationship between the energy difference of the two spin states and frequency:

$$E = h\omega \tag{1.2}$$

where h is Plank's constant. The transmitted energy is called an RF pulse as it is in the radiofrequency range, which is much lower than that which can cause ionization in the body like X-rays and other imaging modalities. This leads to the B_1 field, the magnetic component of the transmitted RF, that is applied perpendicular to the B_0 field in order to produce a sufficiently observable magnetization. A pulse is produced

when an alternating current through a coil passing at the larmor frequency is being turned on and off, creating a "pulse" of RF energy. Although, the energy need not be pulsed and may be left on for some period of time. This causes the perturbed net magnetization vector to precess and be tipped at an angle relative to the direction of the static magnetic field:

$$\theta = \int_0^\tau \gamma B dt \tag{1.3}$$

where τ is the duration of whatever B field is applied (in this case B_1) at the resonant frequency. This is called the flip angle.

Since no spatial information (no transverse component of space) is gained from observing the frequency or phase of the spins precession about the static field, applying variations (gradients) to B_0 can give spatial dependence to phase and frequency. A gradient field is added to the uniform field that is along the axis of the laying body by passing a current through an additional winding within the large magnet coil. To take two dimensional (x,y) images which traverse through the B_0 field (conventionally along z), the RF pulse is applied at the same time as a gradient (in z). The resulting shape of this plane of excited magnetization vectors is determined by the shape of the RF pulse envelope function, which requires RF carrier amplitude modulation and phase modulation. The RF pulse in time will correspond to a range of frequencies (after fourier transformation) which can be selected by the particular shape of the RF. Shaping the pulse envelope to a sinc function, for instance, can produce a square wave that selects a small, well-defined band of frequencies. Spins with these frequencies will be rotated by 90 degrees (for a 90 degree pulse, the angle of which is determined by equation 1.3) while other smaller and greater frequencies near the edges of this band will be rotated by lesser angles as shown in figure 1-1. Where the applied RF frequency is far from the larmor frequency, these set of spins will not rotate at all. Equation 1.4 shows the linear relationship between the frequency of precession at a given z position to the gradient (G_z) along the z axis.

$$\omega(z) = \omega_0 + \gamma G_z z \tag{1.4}$$

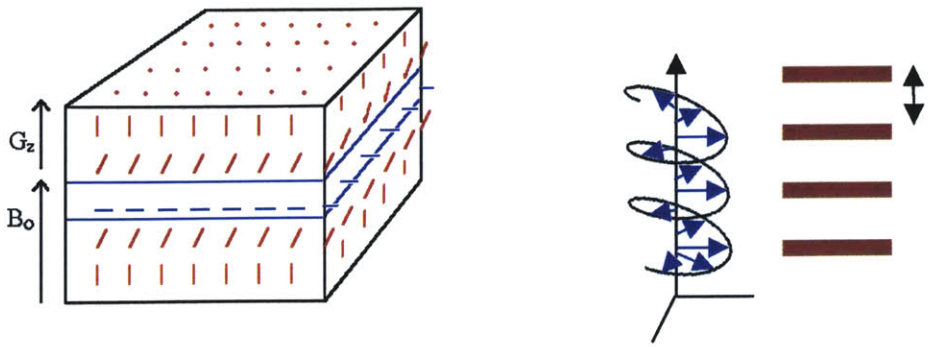

(a) z-gradient

(b) y-gradient

Figure 1-1: All of the small arrows (1-1(b)) or sticks (1-1(a)) represent individual magnetic moment vectors. In (a) a voxel of spins aligns itself with the B_0 field along the z axis. A gradient is also applied with the B_0 field. The small band of frequencies of the spins corresponding to the specific shape of the RF pulse will shape a certain x,y plane of tipped spins. The y axis of these tipped spins is magnified in (b). The vectors show periodically varying phases along the y axis which form a helix, and which can be traced with "blips" or pulses of the y gradient shown as dark bands alongside the helix. The gradient along y tightens the helix and allows for sampling of the spatial frequencies.

Frequency and phase encoding gradients are also applied that cause the B field to vary (usually linearly) with respect to position along the x and y axis. Applying a gradient in the x direction will cause the B field to increase with x. Thus, we can trace where a given group of spins is located in the x direction by measuring their spin frequency during the acquisition of the signal (also called the read-out gradient). The relative phase shifts of different groups of spins that have resulted from the applied gradients since excitation can also be determined by applying a gradient whose timing and strength are chosen according to a desired spatial resolution. During a gradient in the y direction applied before the image acquisition, spins at different y locations spin at different frequencies and acquire different phases (1.3). The magnetization

vectors in space will form a helix along the y axis as shown in figure 1-1(b). Since the phase shifts of spins at a certain y location necessarily match up with spins at another in a well-defined spatial periodicity, the timing of the gradient is kept constant from excitation to excitation. The phase of a magnetization vector can then be set by a phase encoding gradient pulse. After fourier transforming the time and phase domain raw data (in arbitrary units) of a particular voxel in the frequency and phase encoding directions, the frequency and phase of the resulting peak will correspond to the location of the voxel in the brain. The area with respect to time of the pulsed gradient gives information of the image spatial resolution.

Through electromagnetic induction, a precessing magnetic moment in the transverse plane induces a small voltage in a "receive" coil that results in the MR signal (the free induction decay or FID signal). After experiencing these different magnetic fields (pulse sequence) the transverse components die out. The rates at which these moment vectors return to equilibrium direction are what provide image contrast. Since the MR signal from a given voxel is proportional to the density of spins and will have phase (now dependent on location due to the gradients), it is useful to have a well-defined notion of spatial frequency space, or "k-space", to spatially reconstruct an image from k-space to object space through fourier transformation [10]. Phase and frequency are related as shown in equation 1.3, and with a constant gradient in time, the phase induced by a gradient in x, for instance, is $\gamma G_x t$, where t is the duration of the gradient. This is defined as k_x, and each point in the k_x direction corresponds to a sampled point of the signal at a particular time-point during the readout gradient. The same applies to the gradient in y. The units of k are 1/cm, which is analogous to frequency (1/s) when thinking of fourier conjugate variables. One convention fills one row of a kspace matrix at a time with, say 256 points in the frequency encode direction and 128 in the phase encode direction. The y helix is quickly wound and then left in place during the readout by blipping it on before the readout. Each excitation can be performed with a different area of the phase encode gradient so that a different line of k_y can be filled. The phase encode amplitude can be stepped from negative to positive values. In most objects, the signal is largest at

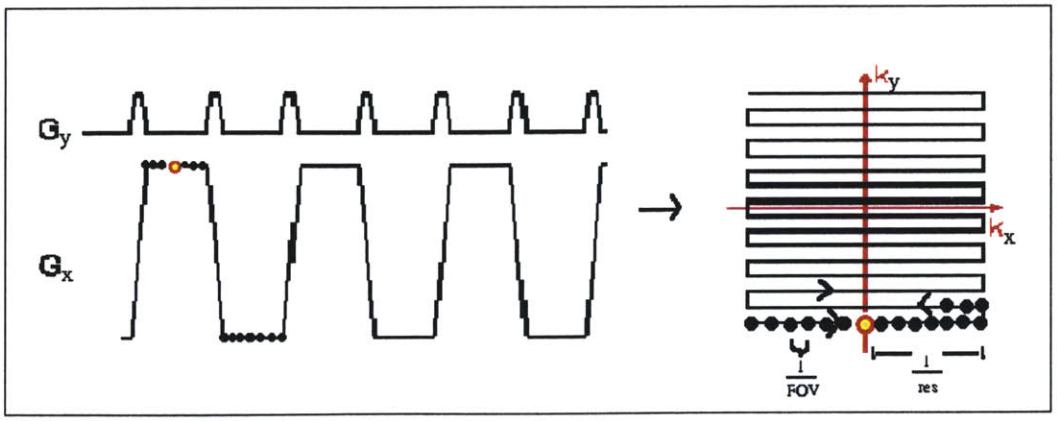

Figure 1-2: Shows the trajectory of kspace that corresponds to the gradients in x and y in EPI imaging. The rapid back and forth traversal of the readout axis in k-space is performed using an oscillating readout gradient. The dots represent points that are collected throughout this traversal while the gradients are on.

the k_x equals zero point, as it is the zero spatial frequency component with the helix (figure 1-1(b)) completely unwound and spins aligned. The image resolution sets the maximum k value (k_{max}=1/res), and therefore also sets the maximum gradient and max time it should be on. The field of view is dependent on the resolution of the k-space. Because phase errors tend to build up over time when going from odd to even lines in kspace, it is important to traverse kspace quickly enough while resetting the phase with each excitation.

Echo Planar Imaging is one technique in which 15-30 images of the brain per second can be acquired [8]. It rapidly cycles between frequency and phase encoding gradients during the usual period when the signal is recorded. This allows all of k-space to be traversed in a single period of acquisition, TR (time to repetition, or time between RF pulses). In modern scanners, the collection of each data line can be as rapid as 300 microseconds. Figure 1-2 shows how the sign of the readout gradient is quickly changed and corresponds to alternating between directions in the kx space. The phase encoding blips bump us up to a different line in k_y.

The recorded signal is therefore shaped by the different phases acquired from the different gradients. It can be manipulated to depend more on either of the following: 1. the time constant T_1 governing the time the longitudinal magnetization component

M_z returns to its equilibrium state M_0 from the spin interactions with surrounding lattice; 2. the time constant T_2 for the transverse component M_{xy} to return to zero from spin-spin interactions; or 3. the density of spins in the sample. This is done through careful application of the B_1 field—the interval (TR) between RF pulses and the time between the pulse and a readout acquisition (TE). The specific relationship between the magnetization vector $M_{(t)}$ and a magnetic field applied is shown in the following empirically determined differential equation (named the Bloch equation [8]):

$$\frac{d\mathbf{M_{(t)}}}{dt} = \mathbf{M_{(t)}} \times \gamma \mathbf{B_{1(t)}} + \frac{(M_0 - M_z)\hat{z}}{T_1} - \frac{\mathbf{M_{xy}}}{T_2} \tag{1.5}$$

where the bold indicates vector quantities that can be analyzed separately in x, y, and z components.

1.2 What can be observed with fMRI

The imaging techniques described above, and EPI in particular, provide images quickly enough to show differences in momentary blood flow throughout the brain. This allows us to map the functions of various regions of interest in the brain, hence *f*MRI, where *f* stands for functional. As described earlier, the MRI signal comes from hydrogen nuclei that are mostly present in water from the blood. Hemodynamic changes due to activation come in two forms: increases in local blood volume and blood flow. Surprisingly, rate of oxygen consumption rises only modestly (e.g. 15-30 percent) due to experimentally induced activation in the brain [9]. There is, however, an approximate 50 percent increase in blood flow. These are experimental values dependent on particular imaging parameters and type of stimulation, but nonetheless show that blood flow increase is greater than oxygen consumption. This mismatch is probably due to decrease in capillary transit time which hampers oxygen extraction [10]. The concentration of deoxyhemoglobin in the venules decreases slightly with increased flow which increases the MRI signal (since the paramagnetic properties of deoxyhemoglobin and the resulting microscopic field gradients dephase the MR signal). The static and dynamic magnetic field changes in Blood Oxygen

Level Dependent (BOLD) experiments cause dephasing of signals which decreases the signal to noise ratio [1] and therefore exhibits poor spatial resolution.

On the other hand, perfusion fMRI techniques focus on the rate of delivery of metabolic substrates during activation. The rate of delivery of arterial blood—cerebral blood flow (CBF)—is often used as a tracking device to determine how the brain functions when activated. Bolus tracking studies with contrast agents do not provide functional or dynamic images of flow, rather they produce maps of agents with low temporal resolution [4] [9]. Also, experiments with intravascular contrast agents are invasive which limit the freedom with which they are used in human studies, and the results may be more sensitive to decreases in CBF than increases [4]. This is useful in measuring ischemia, for instance, but not for measurements of CBF changes with activation in a healthy brain. These types of measurements are important for the assessment of problems with blood delivery and tissue perfusion in the long-term.

1.3 ASL

Arterial Spin Labelling (ASL) is a technique developed for the measuring of local tissue perfusion with MRI [5] that is completely noninvasive and provides relatively high spatial and temporal resolution as compared to many other current functional imaging techniques. ASL gives direct measurements of CBF to a local brain voxel in an imaged slice of interest. The measurement of blood flow begins with a 180 degree radiofrequency (RF) inversion pulse applied to flip the transverse magnetization of the hydrogen molecules in the water of arterial blood before it reaches the imaging slice. The magnetization serves as a label or tag (a diffusible tracer [21]) which flows into tissues in proportion to local CBF. After some delay to allow the magnetically "tagged" arterial blood to be delivered to the slice of interest, a "tag" image is acquired. To reference this image to one where arterial blood is fully relaxed, this procedure is repeated without tagging the blood. These two images are then subtracted, removing static spins in the imaging slice, isolating the relevant signal of arterial blood delivery and ultimately creating a map of brain perfusion.

However, the brain is composed of different types of matter and blood vessels that vary in their direction, size, volume, resulting blood velocity, bifurcation, density, and several other factors. In addition, instabilities in the background signal from water in static tissue can add noise to resulting signal after subtraction. A large variety of ASL techniques have emerged to account for these confounding factors. They are different in how they tag the blood, how the reference or control image is made, and how they account for magnetization transfer effects and transit delays described below.

ASL has branched into two streams: first, continuous (CASL) and then pulsed (PASL) techniques. PASL applies a single spatially selective 180 degree pulse that inverts all spins at once in an inversion slab. In the CASL approach, arterial blood is continuously inverted in the neck before it gets to a slice of interest using a constant, continuous RF power pulse applied in the presence of a constant magnetic field gradient along the flow direction. A continuous RF pulse is actually just an RF field that is applied for a much longer time (several seconds) than a typical excitation pulse [4]. For as long as the RF pulse is applied along with a gradient, an inversion plane is formed (as shown in figure 1-1), where the pulse is on-resonance with the frequency of the blood in the area selected by the gradient (or while ω equals ω_0 (1.4)). When flowing blood crosses this plane, its magnetization is inverted and then a tag image can be acquired further along as described earlier. Since the gradient and the continuous RF pulse are held on and constant throughout the tagging band, the transit time, or duration of the arterial bolus, is experimentally determined. In CASL, a control image is typically acquired with the inversion plane symmetrically above the tagged plane (can be created through off-resonance irradiation or specific slice gradient) so that the blood delivered to the slice of interest is not tagged (see figure 1-3). The subtraction of these images leaves out static tissue and shows the amount of arterial blood delivered to each voxel of the slice in the time delay allotted. However, because the RF pulse is dragged out through time, the resulting subtracted image may be contaminated with magnetization transfer effects. Magnetization transfer effects occur when any off-resonance irradiation (with ω far from ω_0) affects the image slice plane, and when this effect is not completely compensated by having the same effect

present in the control image. After enough time, flowing blood begins to perfuse into surrounding tissues composed of lipids or specific ions, for example, that absorb energy in a broad range of frequencies. During this long off-resonance RF, the tagged blood exchanges magnetization with static tissue and macromolecules within which decreases the steady-state longitudinal magnetization of the "static" spins in the image slice. When the image plane RF is applied to acquire the image, the overall signal acquired is less. This affects the resulting signal in the subtraction image which alters the measurements of the relaxation times near the tissues of interest, and therefore our understanding of this area's physiology and characteristics. These effects depend directly on the amount of time of off-resonance RF irradiation during an imaging sequence repetition interval [17]. Even though control images can have RF pulses that are off-resonance by the same amount as the tagging RF pulse, it is difficult to capture the exact same amount of magnetization transferred to macromolecular spins through blood exchanges in multiple slices.

The amount of integrated RF power delivered during a sequence interval is another way of predicting the magnetization transfer effects. The total energy associated with the RF magnetic field is the time integral over the entire pulse of the power delivered to the system [8]:

$$Energy = \int dt B_1(t) B_1^*(t) \tag{1.6}$$

where $B_1(t)$ and $B_1^*(t)$ are complex conjugates of the applied RF pulse. The greater the integrated power, the greater the possibility of magnetization transfer effects. In order to avoid magnetization transfer and exceeding the limitations of specific absorption rate of RF power (some of which is deposited as heat in the body), it is useful to consider the power associated with achieving a given flip angle (1.3) in a given time for specific slice parameters.

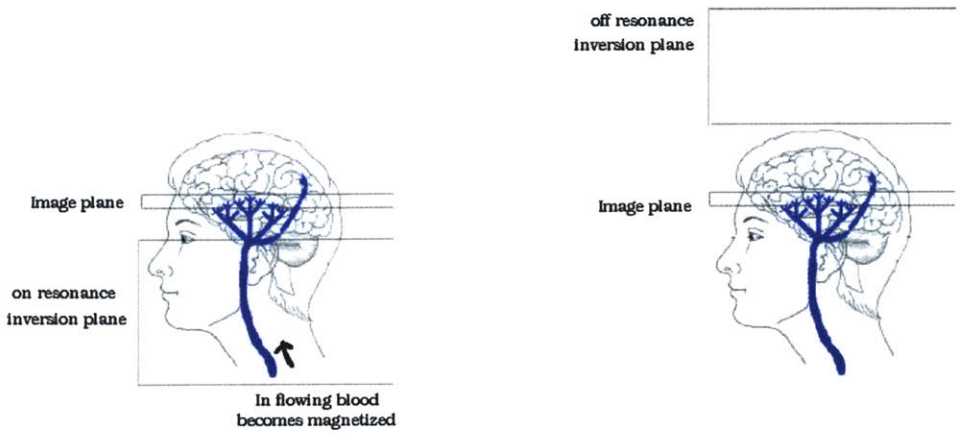

(a) asl-tag

(b) asl-control

Figure 1-3: Figure 1-3(a) shows the tagging plane that inverts the magnetization of in flowing blood originally parallel to the B_0 field. The bolus of magnetized blood then flows towards the plane of interest where an image slice is acquired. Figure 1-3(b) shows the control image acquired symmetrically above the tagged plane so that no in flowing blood is inverted.

1.4 Adiabatic Pulses

Adiabatic inversion allows for maximum inversion to a desired flip angle above a threshold B_1 voltage. For adiabadicity, the RF pulse frequency ω_1 is varied with time, from one side of resonance (ω_0) to the other, where ω_1 has the same relationship to B_1 as equation 1.1 shows for ω_0 and B_0. As $B_1(t)$ is applied perpendicular to B_0, an effective field $B_{eff}(t)$ is experienced by the net magnetization vector $\mathbf{M}$ which can be thought of as the vector sum of B_0 and B_1. In a frame of reference that rotates at the instantaneous frequency $\omega_1(t)$ about the x axis, B_1 seems constant and aligned perpendicular to the modulated z axis (z'), while on z' there seems to be a field combination of B_0 minus B_1. Figure 1-4 shows this relationship in a coordinate system. If the frequency at which B_1 is applied varies with time ($\omega_1(t)$), the magnetization does not actually acquire a phase from its immediate wide precession

that tips it onto the transverse plane, rather it precesses at $\Delta\omega$ (the same offset from equation 1.12 [14]), which is equal to $\omega_0 - \omega_1(t)$ (the resonance offset) [4]. In the adiabatic process, at the start of the pulse, ω_1 is far off resonance ($\omega_1 < \omega_0$), so $\Delta\omega$ is close to resonance, and so B_{eff} is roughly aligned with B_0 . As ω_1 increases, B_{eff} rotates towards the transverse plane until it reaches resonance ($\omega_1 = \omega_0$) and then goes beyond it ($\omega_1 > \omega_0$) for a 180 degree flip angle. The magnetization vector **M** ideally aligns itself with the B_{eff} vector as expected if and only if the rate at which the B_{eff} vector changes orientation is much less than the rate at which the magnetic moment vector precesses about B_{eff}. This precession rate is known as ω_{eff} which is equal to γB_{eff} and is the vector sum of ω_1 and $\Delta\omega$ in the rotating frame . This condition is known as the adiabatic condition [20]:

$$\frac{d\alpha}{dt} \ll \omega_{eff} \tag{1.7}$$

where $\frac{d\alpha}{dt}$ is the angular velocity or sweep rate of B_{eff} and can be expressed vectorially as:

$$\tan\alpha(t) = \frac{\omega_1(t)}{\omega_1(t) - \omega_0} \tag{1.8}$$

The trajectory of the ω_{eff} vector is the trajectory of the adiabatic pulse and can predict the trajectory of the magnetization vector [16]. The vector magnitude is:

$$\omega_{eff} = \sqrt{\omega_1^2 + \Delta\omega^2} \tag{1.9}$$

The flip angle as shown by figure 1-4 is no longer determined by equation 1.3, rather it depends on the shape of the pulse and the sweep rate. Because in general an RF field is much weaker than B_0, the rate at which **M** precesses around B_1 (which is effectively B_{eff} after enough rotation) is correspondingly slower (1.1). But if we wait long enough, the magnetization will rotate around B_1. Silver et al. shows that after enough time, given certain boundary conditions, a sech function will invert

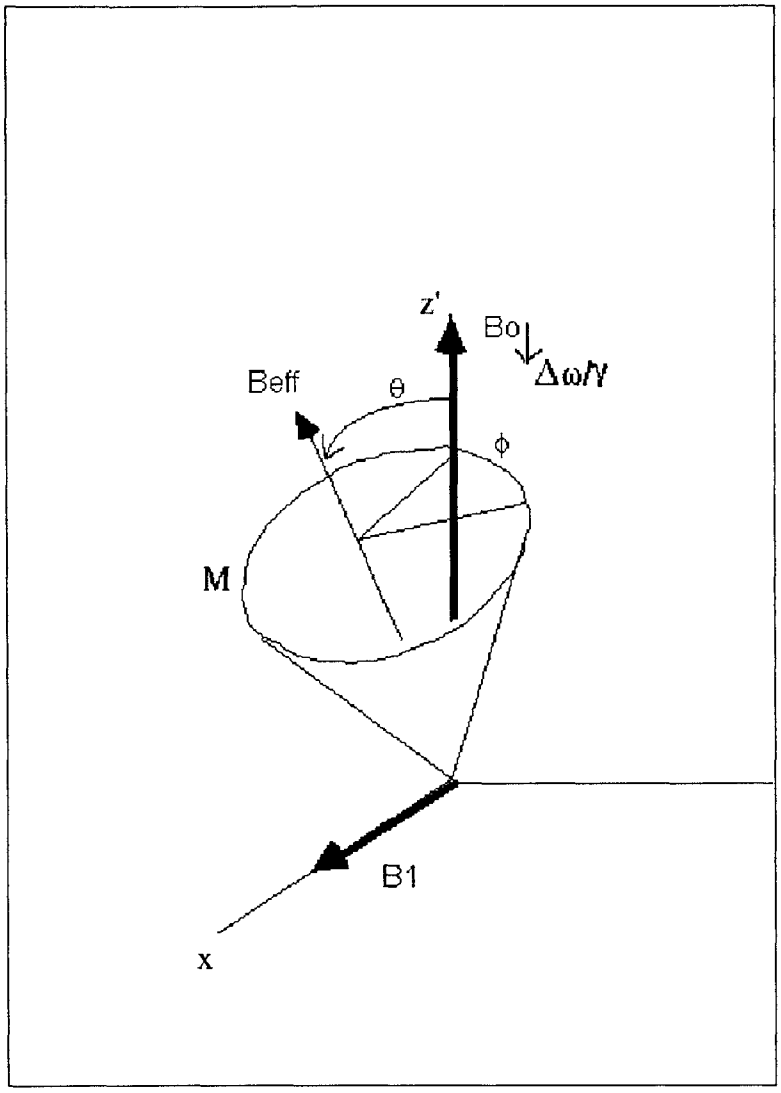

Figure 1-4: Shows B_{eff} changing orientation from initially along B_0 to near B_1 for a 90 degree flip angle θ, which is essentially α. **M** follows B_{eff} and precesses about it as shown. $\phi = \omega_{eff} t_1$, where t_1 is the time the B_1 is applied. When $\omega_1(t)$ reaches ω_0, the B_{eff} is along the B_1 axis and is equal to B_1, and the magnetization follows it reaching a 90 degree flip angle.

the longitudinal magnetization fully over all frequencies [19]. If enough time is not allotted to the duration of the sech function, then inversion is incomplete. Implicit in the adiabatic condition is that no relaxation can occur during the process, i.e. the magnetization should not be allowed to return to its equilibrium state. To reduce initial precessesion about the effective field once B_1 is applied, and thus momentary relaxations, the starting angle α_0 of the effective field should be as small as possible, and the change in α_0 thereafter should be small as well. This makes sure that the magnetization is given enough time to align (or relax back, after initial precession) with the effective field and not precess so much as to partially revert to its equilibrium state and produce inefficient inversion. If the change in α is not kept to a minimum, then the precession will increase in diameter as the combination of ω_{eff} and $\Delta\omega$ will have greater instantaneous disparity and the magnetization vector will not be able to fully align with the effective field. With slow movement of B_{eff}, or, effectively, slowly sweeping through frequency ($\omega_1(t)$), **M** will be able to precess many times around B_{eff} for each time point, so it will form a tight cone around B_{eff} (Figure 1-4 shows the phase ϕ of this cone) and follow it towards the x axis and beyond [4].

Another way to achieve adiabatic inversion besides a slow frequency sweep is to use a sufficiently high B_1 amplitude. Using sufficiently high RF amplitude with adiabatic pulses produces near-perfect inversion and assures the adiabatic condition as can be seen by plugging in high values for B_1 and its corresponding ω_1 in equations 1.9 then 1.7. In general, at higher magnetic field strengths, the ASL signal-to-noise ratio (SNR) increases because of longer duration of proton magnetization in blood and tissue [11]. However, it is important to use a suitable combination of B_1 amplitude and frequency sweep, and the specific RF pulse shape determines the efficiency and distribution of RF energy in the sample.

1.5 Pulse Shapes

Earlier it was shown that if an RF pulse is amplitude-modulated by a sinc function, its frequency selectivity becomes a sharp boxcar function. However, sinc pulses must

be cut off in time, which inevitably produces finite transition bands and ringing in the slice selection and intrinsic B_1 inhomogeneity. Another function which is commonly used for greater B_1 homogeneity and inversion efficiency is the adiabatic hyperbolic secant (sech) function proposed by Silver, Joseph and Hoult in 1985 [19]. One form of this function is an amplitude and phase modulated pulse:

$$B_1(t) = B_{1_0}(sech\beta(t - t_{center}))^{1+i\mu} \tag{1.10}$$

where β (pulse length paramter), and μ (side to width paramter) are constants and this is a direct complex solution of transformations of equation 1.5 that neglect relaxation effects [19]. In order to obtain an understandable frequency domain spectra from this solution, a coordinate transformation can be made where a phase correction is applied and the real component can be analyzed. The real amplitude then becomes:

$$B_1(t) = B_{1_0}(sech\beta t) \tag{1.11}$$

with frequency offset:

$$\Delta\omega = -\mu\beta \tanh \beta t \tag{1.12}$$

After plugging in this solution into equation 1.5 we arrive at an equation showing the relationship between the magnetization vector and B_1 amplitude. Silver et al. shows how above a μ (side to width parameter) value of 2 and for a value of amplitude B_{1_0} greater than or equal to $\mu\beta$, the slice selection bandwidth of the hyperbolic secant pulse is given by $BW = \pm\beta\mu$. Also, under these conditions, the B_{1_0} term in the resulting equation drops out, leaving the longitudinal magnetization completely independent of the amplitude of the applied field B_1, making it resilient to inhomogeneities. The minimum B_{1_0} value was determined after applying boundary conditions to the solution in order to have magnetization efficiently inverted over all frequencies.

The sech RF pulse shows vast improvement from the conventional sinc 180 degree inversion pulse especially with respect to tolerance to RF field inhomogeneity and

bandwidth. The conventional pulse provides an acceptable inversion only over a relatively narrow resonance offset bandwidth (95 percent inversion over plus/minus $0.2B_1$) [18]. If an RF field strength is set at, say, 20 kHz, a conventional 180 degree pulse will reduce the bandwidth to 4 kHz, which cannot cover the 5-kHz proton range (10 ppm) of a 500-MHz spectrometer. For a variety of different nuclei, chemical shift ranges may require large bandwidths. Other adiabatic pulses that also achieve a wide band of inversion with moderate RF power and are tolerant to B_0 and B_1 inhomogeneities above a minimum B_1 are the hyperbolic tangent (tanh) and WURST functions [18]. The tanh pulse equation is as follows:

$$B_1(t) = B_{1_0} \tanh\left(\zeta\left(1 - \frac{2t}{T_p}\right)\right) \tag{1.13}$$

where ζ equals 10, T_p is the pulse length, time goes from negative one-half of T_p to postive one-half T_p. The WURST equation is :

$$B_1(t) = B_{1_0}\left(1 - \left|\sin\left(\frac{\pi t}{T_p}\right)\right|^n\right) \tag{1.14}$$

where n is an adjustable positive integer which controls the attenuation of the amplitude shape at the ends of the pulse.

A family of not entirely adiabatic pulses proposed by Smith et. al. [18] also produce broadband, high-power inversions are called Broadband Inversion Pulses (BIP). These are typically shorter pulses that cannot be represented by a formula, rather have phase functions as piecewise cubics with coefficients optimized for a desired pulse length, resonance offset, and B_1 inhomogeneity compensation. Other pulses such as the FOCI (Frequency Offset Corrected Inversion) pulse introduced in 1996 by Odridge et. al. are tailored for optimal, sharp slice selection, but do not achieve efficient inversion over a broad bandwidth as do the BIP and other adiabatic pulses mentioned. Most of the adiabatic and BIP pulses have slow enough sweep rates to acquire a desired inversion in blood, but can fall short when taking into account the faster signal decay in tissue due to spin-spin interactions (T_2). Broadband inversion and RF field inhomogeneity is not only important for efficient excitation in blood,

but also for suppression of static tissue signal in ASL.

1.6 Background Suppression

When static tissue varies from image acquisition to image acquisition, either because of motion, frequency changes, or even machine instability, desired blood signal is lost and erroneous signal corrupt the subtraction images. In particular, magnetic field fluctuations between acquisitions in k-space lead to extra phase noise in true 3D ASL images that are sensitive to individual k-space data phases.

For the purpose of attenuating static tissue signal, multiple inversion recovery (MIR) suppression was first introduced by Dixon et al. in 1990 through angiography experiments [6]. They showed that if static tissue is saturated in the region of interest (ROI) with a selective 90 degree pulse (called presaturation) and then inverted 180 degrees before the tagged blood reaches it, the final static tissue signal reduces to near 0 and the labeled blood signal is unaffected. This can be shown theoretically. If the signal from labeled blood is termed S_{bl} and unlabeled blood is termed S_{bu}, the ASL signal is the difference between the two. If blood is labeled an insignificantly small amount of time after presaturation and then inverted time a after presaturation for image acquisition, the subtraction signal can be had as follows:

$$\text{for} \quad t < a$$

$S_{bu} = 1$ (magnetization assumed to be aligned with B_0 field)

$S_{bl} = 1 - 2e^{-t}$ (magnetization recovery after tag is exponential as per equation 1.5)

$S_{bu} - S_{bl} = 2e^{-t}$

$$\text{for} \quad t \geq a$$

$S_{bu} = 1 - 2e^{-(t-a)}$ (magnetization of unlabeled blood recovers after inversion)

$S_{bl} = 1 - 2e^{-(t-1)} + 2e^{-t}$

$S_{bu} - S_{bl} = -2e^{-t}$

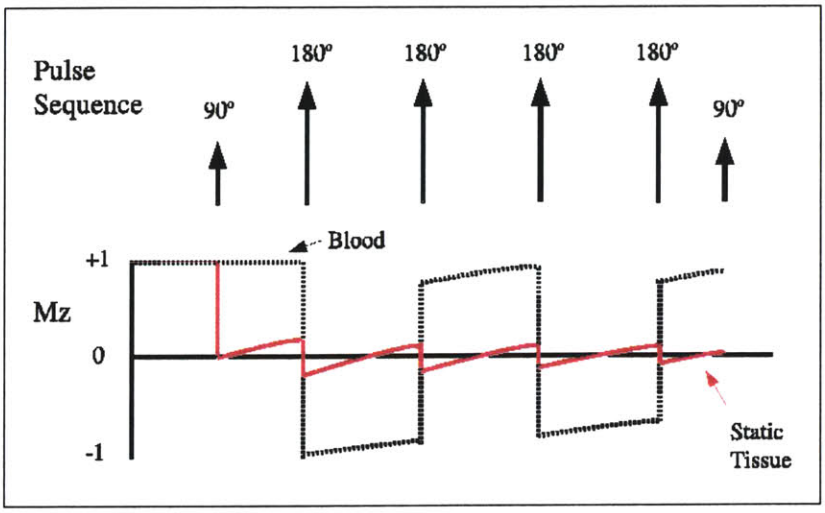

Figure 1-5: Shows the timing of the multiple inversions and the corresponding effect on the magnetization of static tissue and inflowing blood. The longitudinal magnetizations of each are assumed to initially be aligned with the B_0 field along the positive z axis (+1).

Even though the signs of the two subtraction solutions are different and the image acquisition inversion affects both labeled and unlabeled blood, the extra inversion at a has no real effect on the difference value which determines the overall signal. In the same way, the final subtraction signal is not affected regardless of the number of extra inversions after presaturation. The only change that will result from the number of inversions is the sign of the subtraction value [6]. With more inversion pulses applied, static signals from tissues with different T1 can be synchronized.

To account for variations in the static and RF fields which affect the quality of the MIR suppression, Mani et al. [13] then applied a sequence of four, wide bandwidth adiabatic sech pulses to achieve an accurate suppression of the longitudinal static tissue signal over a broad range of T1 values. Figure 1-5 shows a sequence with the four different non-selective inversions after the selective presaturation pulse and the corresponding exponential magnetization recovery which results in low final static signal. When part of the labeled blood is inverted and part is not, either because of the preciseness in selectivity of the pulse or capacity of a coil used for slice selection, blood signal is lost. This gives incentive for using non-selective inversion pulses that invert both labeled and unlabeled blood after presaturating the ROI.

Since the ASL signal change is typically less than one percent of the background signal intensity, background suppression using multiple inversion pulses can be used to greatly attenuate the background signal and hence improve the quality and robustness of ASL. As the number of pulses used increases, the background suppression can be optimized for suppression of better than 100x across a wide range of T1 [13]. With perfect inversion pulses, the background suppression should have no effect on the ASL signal, but even small imperfections can attenuate the ASL signal when a large number of inversion pulses are used. Understanding of this inversion inefficiency is important both for optimizing sequences and for absolute quantification of the ASL results.

1.7 Purpose

The goal of this study was to analyze the degree of signal that is lost in background suppression using pulses that have been shown to achieve efficient inversion over practical inhomogeneities in B1 and B0. Using a wide range of experimental parameters, simulations of the hyperbolic secant pulse (*sech*), hyperbolic tangent (*tanh*), WURST-5, and Broadband Inversion Pulse were obtained in order to determine an optimal range of values that provide the most efficient inversions. These parameters for the hyperbolic secant and hyperbolic tangent pulses were then tested *in vivo* through two and three dimenional image acquisition and the results compared to theoretical inversion efficiency values. Factors such as the amount of integrated power delivered with these pulses were also explored. Effects of T_1 and T_2 decay were also considered.

Chapter 2

Methods

The methodology described here consists of computer simulations of aforementioned pulse shapes and corresponding inversions of magnetization, as well as experimental trials of some of these shapes on one healthy subject.

2.1 Simulations

Using numerically integrated Bloch equations for calculations of adiabatic inversion as described in [12], four different B_1 pulse shape functions were explored for blood and tissue T_1 and T_2 . We ran simulations of these pulses to find an optimal range of pulse parameters that produced the most efficient inversions. The formulae for these functions were gathered from Smith et al. ([18]) and show the parameters unique to each pulse. Three are given in section 1.5 (BIP pulse has no explicit function).

Figure 2-1 shows the shapes of the amplitude and phase for these pulses at specific parameter values, including the BIP pulse. The BIP pulse was based on the discontinuous phase shifts of composite pulses [18]. As with composite pulses, there is no underlying analytical functional form. Over various bandwidths, successive downhill Monte Carlo optimizations of a rectangular grid of possible points in offset and RF field strength produced a list of phases fitted to a pulse template with desired length and inversion performance. This phase list for the BIP pulse in terms of the normalized pulse length was approximated as a piecewise cubics phase function:

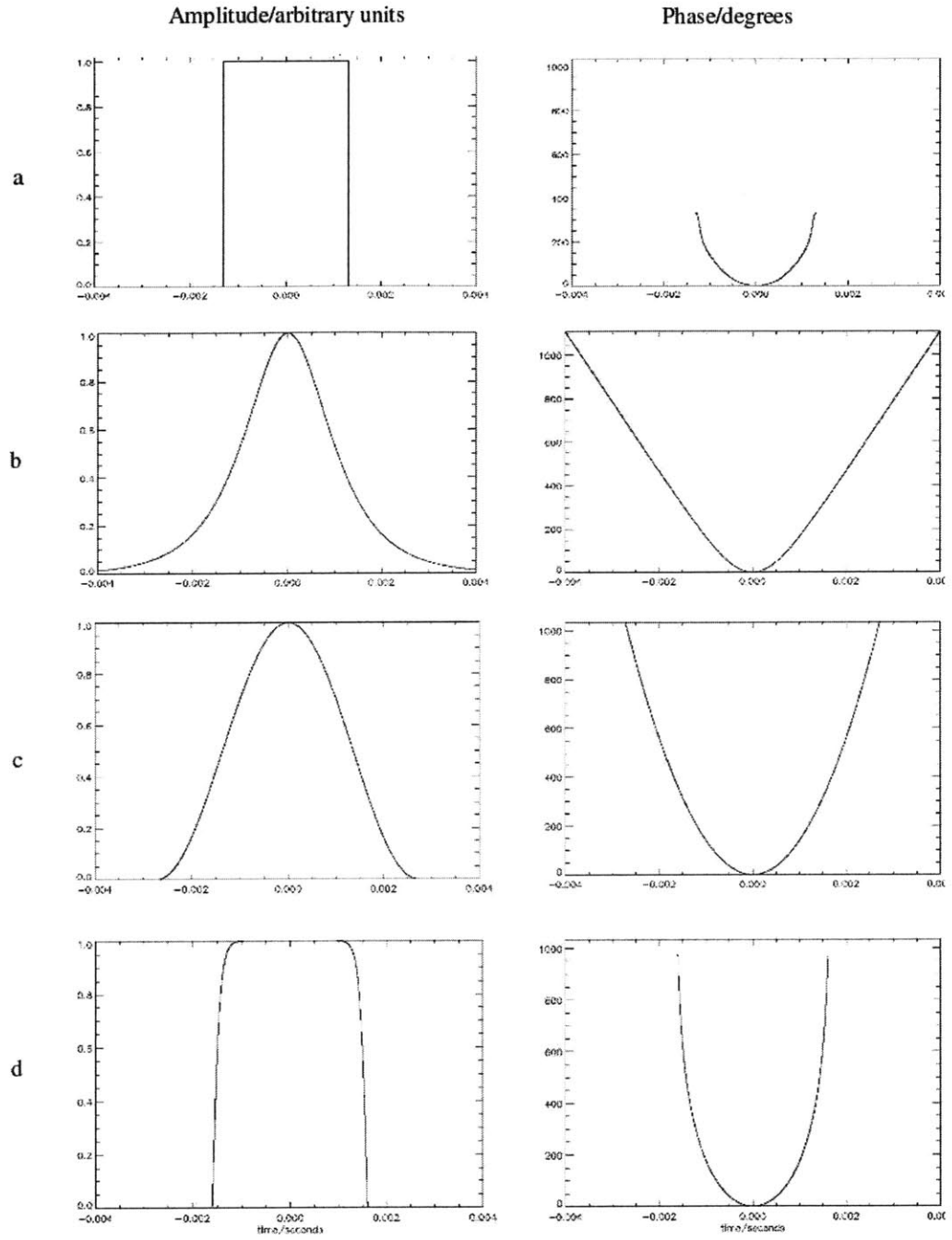

Figure 2-1: Pulse amplitude and phase for BIP, hyperbolic secant, WURST, hyperbolic tangent. a) BIP-720-50-20 amplitude and phase. Phase approximation for BIP pulse of length 720 degrees (2.6 ms for our B1 of .18Gauss), with inversion optimized for a range of $\pm 50\%$ offset ($\pm$ 383.13 Hz offset for our 766.44 Hz B_1 pulse), and optimized for 20% of RF field tolerance (from 0.124 G to 0.23 G for our peak B_1 of 0.18 G). Time goes from negative half of the pulse length to positive half. There were 5000 points sampled at a step size of dt=2.6/5000. b) The hyperbolic secant amplitude and phase are shown for a pulse length of about 8 ms, a μ of 4.4889, and β of 1250. c) The WURST amplitude and phase are shown for a pulse length of 5.4328 ms, and n=2. d) The hyperbolic tangent pulse amplitude and phase, with pulse length of 3.2108 ms.

$$\text{BIP:}\phi(degrees) = a_0 + a_1 \mid \tau \mid + a_2 \mid \tau \mid^2 + a_3 \mid \tau \mid^3; \qquad -10 \leq \tau \leq 10 \qquad (2.1)$$

where a_{0-3} are empirically determined coefficients for this approximation and the normalized length is τ=$10t/(T_p/2)$; $\mid \tau \mid < 10$, where T_p is the pulse length, and time t goes from negative $T_p/2$ to positive $T_p/2$. Of the BIP pulses that Smith et al. presents, the BIP-720-50-20 seemed most optimal for our purposes, which stands for a pulse length of 720 degrees and an optimization for $\pm$ 50 % resonance offset and for $\pm$ 20 % RF field inhomogeneity tolerance. At a peak RF amplitude of 0.18 Gauss, this translates to a 2.6 ms pulse with a offset correction and tolerance from 0.124 G to 0.23 G. The amplitude function was held constant. The actual phase list for increments of from 0 to 10 was gathered from Smith et al. [18] and was pieced together to form the RF pulse shape and phase shown in figure 2-1.

Simulations assumed a peak RF amplitude of 0.18 Gauss and a range of off-resonance frequencies from 0 to $\pm$ 400 Hz. With this offset range and at least $\pm$ 20 % RF tolerance, several different ranges of parameters were explored for each pulse to determine the values that provided the most efficient inversions of blood and tissue magnetization (using blood T_1 and T_2 of 1.4 and 0.25 seconds respectively, and tissue T_1 and T_2 of 1.2 and 0.08 seconds respectively). For the BIP pulse, the pulse length was the only parameter. Since $T_p = 2/(B_1 * 4258)$ for a 720 degree rotation of any non-adiabatic pulse, where 4258 is 10^{-4} times the gyromagnetic ratio for hydrogen, we varied the B_1 value from 0.1 to 0.22 Gauss. We then looked for a pulse length that gave the smallest squared error from a perfect 180 degree inversion over the given offset range for blood and tissue magnetization. For the hyperbolic secant pulse, the simulations ran through a range of μ values from 2-10, and β values from 500s-1 to 3000s-1. The hyperbolic tangent pulse also only had its length as a variable parameter and so we attempted values from 100 μs to 10 ms. This same range of pulse length values was tried for the WURST pulse, including values for n from 1 to 5. The same range of RF deviation from peak value of 0.18G was used with each pulse for each

different combination of parameters. The best parameter ranges were determined by looking at the least squared error from perfect inversion for each pulse, and the power distribution of each was also examined.

2.2 2D *In Vivo* Measurements

Experimental measurements of inversion efficiency were performed on a 3.0 Tesla GE VH/i scanner using the product head coil. The FAIR labeling method was used in a single-slice Echo Planar Imaging experiment, carried out with a TR of 4 s and a TE of 25 ms in an axial slice through the superior part of the lateral ventricles. A control slab of 2 cm was used and labeling was performed with a 40 cm slab to avoid labeling of blood spins far outside the homogeneous regions of the magnet and head coil. Pairs of label and control images were acquired both with and without four closely spaced pulses applied immediately before image acquisition with a 20 cm imaging slab to determine differences in pulse efficiency. These were applied along with a crusher gradient to avoid artifacts. Based on simulation values obtained for maximum inversion for a bandwidth of approximately 800 Hz, a hyperbolic tangent pulse with length of 3.2108 ms was used and the following three combinations of μ and β pairs for hyperbolic secant pulses were tried: 4.4899, 1250; 2.2445, 2500; 8.9778, 625. Perfusion measurements were averaged over 25 repetitions.

Pairs of label and control images were then acquired with and without four optimally timed hyperbolic tangent pulses in a realistic FAIR background suppression strategy. Each of these measurements was averaged over 15 repetitions.

The ratio between the two whole-brain averaged perfusion measurements (with/without four pulses) was used as an indicator of inversion efficiency. An RF field of approximately 0.18 Gauss was used but the RF nonuniformity in the brain at 3 Tesla is typically less than 30%.

2.3 Hyperbolic Secant 3D *In Vivo* Background Suppression Measurements

Three dimensional image acquisition was also performed on a 3.0 Tesla GE VH/i scanner using the product head coil. A partially suppressed continuous ASL preparation with a post-labeling delay of 1s was placed before a stack of spirals volumetric acquisition. Eight shots were required to encode an entire image through spiral fast Spin Echo sequence. Pairs of label and control images were acquired both without and with 6 closely spaced hyperbolic secant or hyperbolic tangent pulses applied immediately after the end of labeling. The difference between the two perfusion measurements was used as an indicator of inversion efficiency. An RF field of approximately 0.18 Gauss was used. Based on simulation values obtained for maximum inversion for a bandwidth of approximately 800 Hz, the following five μ and β pairs were tried for the hyperbolic secant pulse: 3,1400; 4,1400; 5,1400; 4,1000; 4,1800. A pulse length of 3.21 ms was used for the hyperbolic tangent pulse, also based on the simulation results.

Chapter 3

Results

This chapter collects all of the results from the simulation and experimental studies outlined in Chapter 2.

3.1 Simulations

Optimal parameter ranges were found to be similar for both tissue and blood T_1 and T_2 for all pulses, although inversion achieved in blood is slightly better (about 3%) because of longer T_2. Figures 3-1- 3-4 show examples of contour plots for simulated inversion efficiency as a function of different pulse parameters for the *sech* pulse and the WURST pulses (the tanh and BIP pulses only had one parameter to vary). Figures 3-1 and 3-3 are at the center frequency, where the largest inversion is expected, and figures 3-2 and 3-4 are at $\pm$400 Hz offset. Figure 3-1 shows largest magnetization inversion for low μ and high β values just bordering on adiabaticity. Sweeping too rapidly through frequency violates the adiabatic condition but sweeping too slowly adds T_2 decay during the inversion. Figure 3-3 shows similar phenomena with low n values. For the *sech* pulse, an optimal range for maximum inversion was found near values of 4 for μ and 1250 for β with 400Hz offset (figure 3-2). At the same offset frequency, an optimal n of about 3 and a pulse length of about 5 ms gave the most efficient inversion for the WURST pulse (figure 3-4).

After optimal pulse parameters were chosen, the root mean squared inversion error

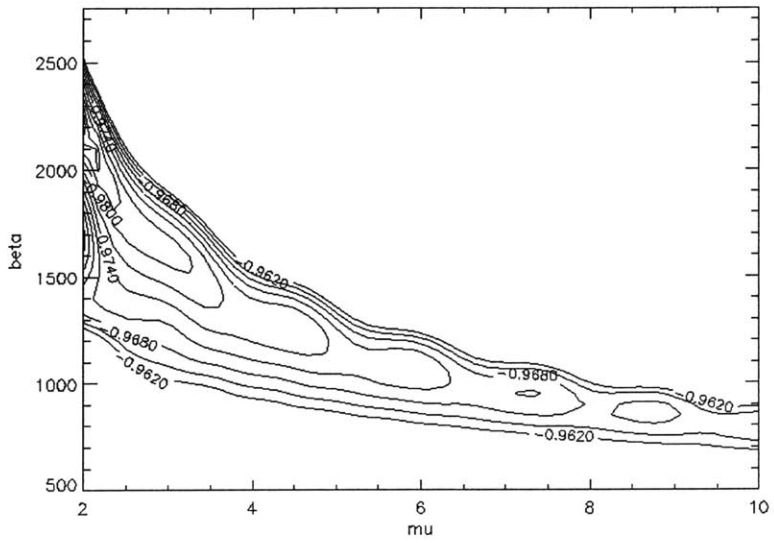

Figure 3-1: Simulated magnetization after inversion with *sech* pulse for spins at 0 Hz frequency offset and with T_1 and T_2 values of 1.2 and 0.08 s typical of brain tissue.

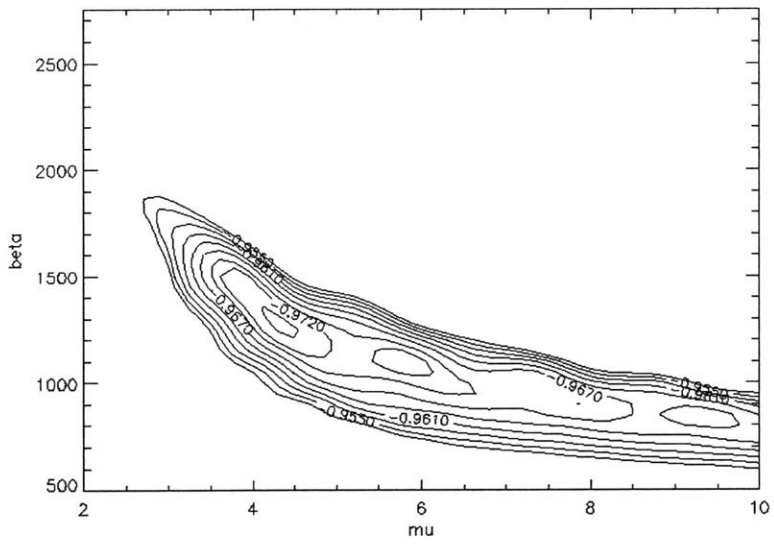

Figure 3-2: Simulated magnetization after inversion with the *sech* pulse for spins at $\pm$ 400 Hz frequency offset and with T_1 and T_2 values of 1.2 and 0.08 s typical of brain tissue.

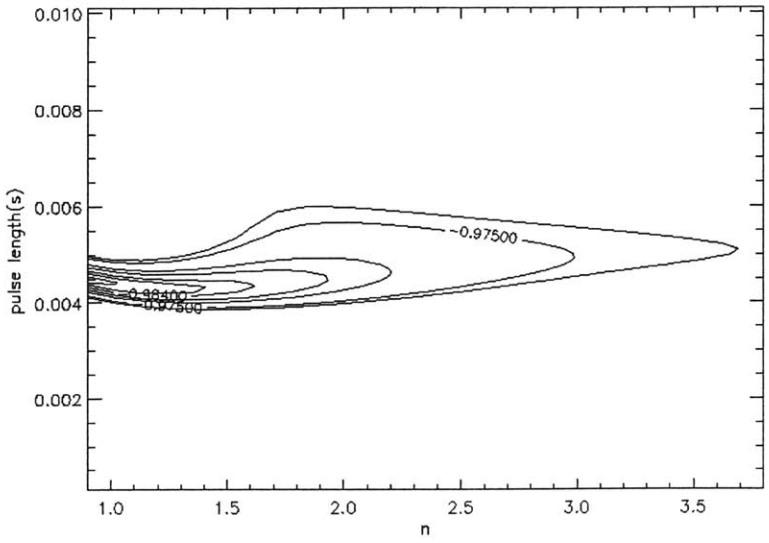

Figure 3-3: Simulated magnetization after inversion with the WURST pulse for spins at 0 Hz frequency offset and with T_1 and T_2 values of 1.2 and 0.08 s typical of brain tissue.

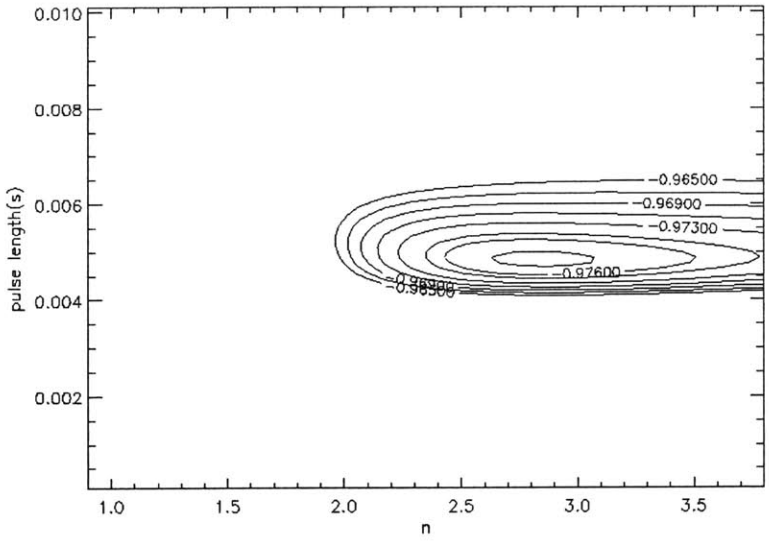

Figure 3-4: Simulated magnetization after inversion with the WURST pulse for spins at 0 Hz frequency offset and with T_1 and T_2 values of 1.2 and 0.08 s typical of brain tissue.

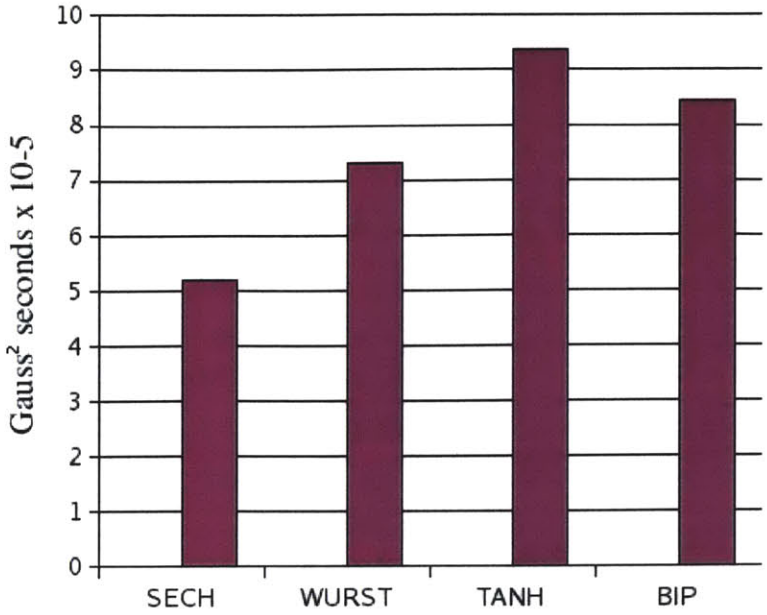

Figure 3-5: Power deposition associated with each pulse.

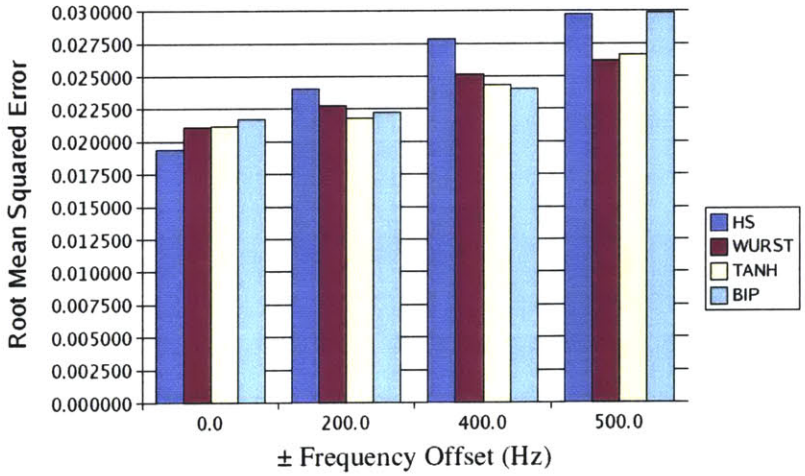

Figure 3-6: Simulated error in tissue inversion at different frequency offsets for all pulses.

across the range of B_1 and B_0 variations studied was small and comparable for the different pulse types, but the tanh pulse generally performed slightly better than the others (figure 3-6). The integrated RF power of the optimal tanh pulse was slightly higher than for the sech pulse, however (figure 3-5), with parameter values optimized for 400Hz offset. Because of its excellent performance, the tanh pulse was chosen for

comparison to the commonly used *sech* to study their efficiency *in vivo*.

3.2 *In vivo* Measurements

Examples of FAIR perfusion images acquired with and without the application of four inversion pulses are shown in figure 3-7. Four inversion pulses caused a decrease in signal of between 10 and 15% for optimal pulse parameters of the *sech* and tanh pulses. Poor pulse selection by slight changing of pulse parameters was disastrous, especially if adiabaticity was lost. In general the results of simulations and *in-vivo* measurements were in good agreement (figure 3-8). Table 3.1 includes efficiency values from figure 3-8 for added reference.

Frequency Offset	Tanh	Sech (8.9,625)	Sech (2.2,2500)	Sech (4.49,1250)
+/- 0 Hz	0.919	0.828	0.726	0.911
+/- 400 Hz	0.896	0.825	0.616	0.904
Experimental	0.870	0.820	0.555	0.974

Table 3.1: Efficiency values for unsuppressed scheme: four pulses applied before acquisition.

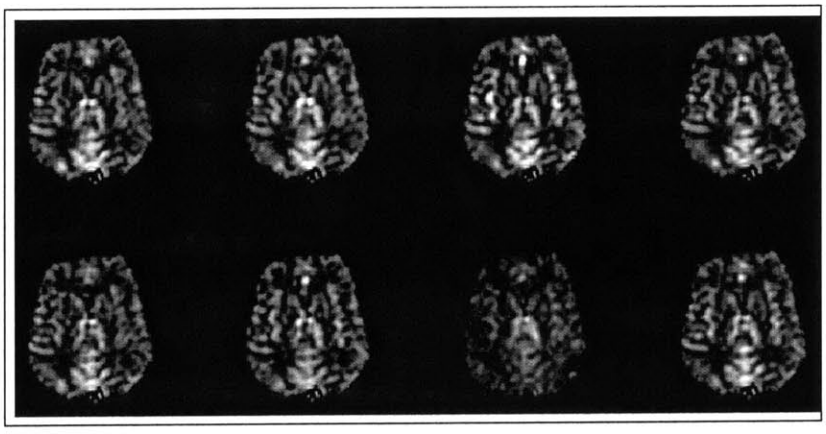

Figure 3-7: ASL perfusion images from one slice acquired without (top row) and with (bottom row) four pulses of the following type and order: tanh, *sech*(8.9,625), *sech*(2.2,2500), *sech*(4.49,1250).

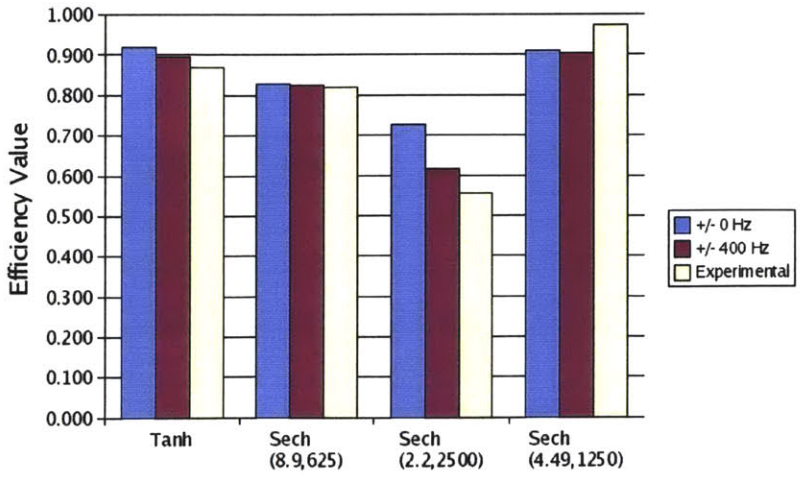

Figure 3-8: Theoretical vs. experimentally acquired efficiency using four different pulses applied four times before image acquisition: hyperbolic tangent and three hyperbolic secant pulses with μ and β values listed respectively.

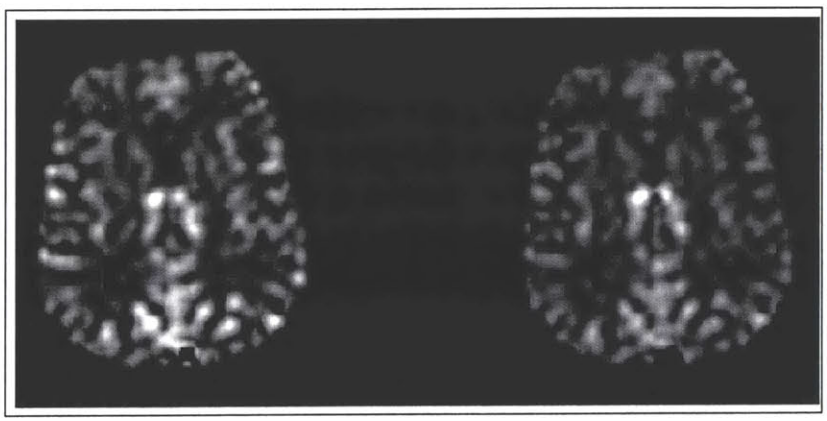

Figure 3-9: ASL perfusion images from one slice without (left) and with (right) four tanh pulses optimally timed for background suppression.

When pulses were spread out over time in an optimized background suppression sequence, similar inversion efficiency was achieved (figure 3-9). This four-pulse background suppression attenuated all brain signal to less than 1% yet preserved 85% of the ASL signal.

The six-pulse background suppression reduced the measured perfusion signal in the 3D acquisition by 13-48% (table 3.2, figure 3-10). Inferred single pulse inversion efficiencies are consistent with our simulation values for blood relaxation times. These results, however, are only for one slice. Other slices containing mostly white matter

unexpectedly show more signal with the six pulses than without. Recent studies with this continuous arterial spin labeling have shown systematic error due to magnetization transfer effects in white matter [3] [7]. This led us to doubt the accuracy of the perfusion measurements in slices with mostly white matter and is precisely what compelled us to pursue the simpler 2D FAIR approach concurrently. The pulsed FAIR experiment allowed detection of smaller changes in the different pulses which agree with the simulation results, and which could not be as accurately detected in the continuous 3D labeling method.

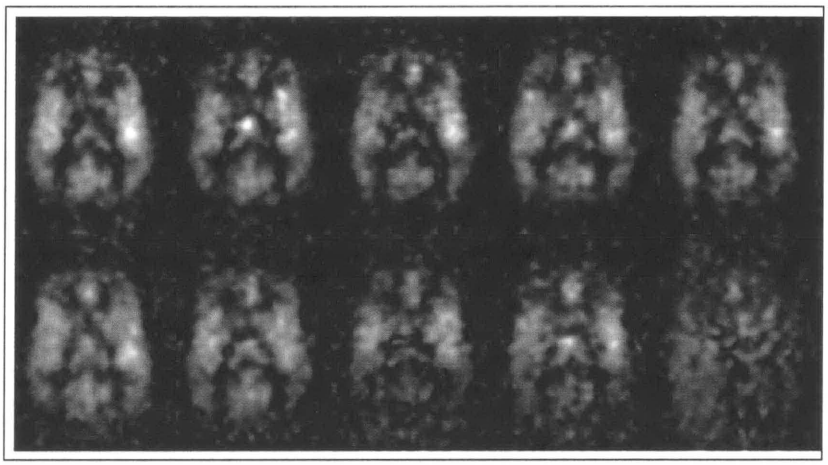

Figure 3-10: ASL perfusion images of one slice from the 3D volume acquisition without (top row) and with (bottom row) 6 sech pulses with μ and β of 3/1400, 4/1400, 5/1400, 4/1000, 4/1800 from left to right.

Mu	Beta	6 Pulses	1 Pulse
3.0	1400.0	0.873	0.978
4.0	1400.0	0.869	0.977
5.0	1400.0	0.773	0.958
4.0	1000.0	0.837	0.971
4.0	1800.0	0.622	0.924

Table 3.2: Experimental six-pulse and single-pulse *sech* efficiency values for different μ and β.

Chapter 4

Discussion

The two dimensional acquisition results indicate that with optimal inversion pulses, ASL signal loss is only 10-15% even when 4 or 6 pulses are employed at optimal pulse parameters. Since prior studies [22] have indicated a similar reduction in noise using background suppression, even when very cooperative normal volunteers are studied, our results provide additional support for the benefits of background suppression in ASL studies.

The two dimensional acquisitions acquired with the FAIR method required large enough labeling slabs to invert as many spins in the brain as possible in order to subtract out static spin signal with the slice-selective control pulse. Some spins outside the brain, however, may contaminate the signal in the acquired image if the imaging slab is large enough or if the TR is small enough. Possibly increasing the TR between repetitions would prevent this signal contamination.

The three dimensional acquisitions suggest that in slices with large quantities of white matter, broadband frequency absorption occurs producing magnetization transfer effects that may leave residual signal from previous acquisitions in subsequent images. Nonetheless, in slices without this notable signal contamination, background suppression seems to be remarkably efficient with as many as six inversion pulses.

While our simulations suggest slight advantages of certain pulse shapes over others, each of the adiabatic pulse designs studied could be optimized for efficient use in background suppressed studies. Optimization generally found a maximum effi-

ciency when the frequency sweep of the adiabatic pulse was just slightly slower than that needed to achieve the adiabatic condition. Using pulses with high adiabaticity decreased efficiency because of increased T_2 decay during inversion.

The efficiency values obtained experimentally mostly agree with theoretical values indicating that the dynamics of the ASL signal were largely governed by T_2 and T_1 and the block equations. Attention to inversion pulse selection is important for assuring high efficiency because both excessive RF amplitude and insufficient RF amplitude can cause strong attenuation of signal.

Although there seems to be a limited optimal range of pulse parameters for the pulses studied, the results demonstrate overall high efficiency of adiabatic pulses and background suppression with up to six pulses. This supports the use of background suppression for accurate quantification of perfusion in further research and clinical studies.

Bibliography

[1] Aguirre GK, Detre JA, Zarahn E, Alsop DC. Experimental design and the relative sensitivity of BOLD and perfusion fMRI.Neuroimage. 2002 Mar;15(3):488-500.

[2] Albert MS, Cates GD, Driehuys B, Happer W, Saam B, Springer CS Jr, Wishnia A. Biological magnetic resonance imaging using laser-polarized 129Xe. Nature. 1994 Jull 21; 370(6486):199-201.

[3] D. Alsop, C. Bazelaire, G. Duhamel. *In Vivo* Imaging of an Inhomogeneous Component of Magnetization Transfer in Human White Matter. International Society for Magnetic Resonance in Medicine: Twelfth Scientific Meeting and Exhibition. 2004 May 15-21;(2324)

[4] Buxton, Functional Magnetic Resonance Imaging: Principles and Techniques, Cambridge University Press, Ch: 4, 7, 15 (2002).

[5] Detre JA, Zhang W, Roberts DA, Silva AC, Williams DS, Grandis DJ, Koretsky AP, Leigh JS.Tissue specific perfusion imaging using arterial spin labeling.NMR Biomed. 1994 Mar;7(1-2):75-82. Review.

[6] Dixon Wt, Sardashti M, Castillo M, Stomp GP, Multiple Inversion Recovery Reduces Static Tissue in Angiograms. Magn Reson Med. 1991 Apr;18(2):257-68.

[7] D.M. Garcia, G. Duhamel, D.C. Alsop, The Efficiency of Background Suppression in Arterial Spin Labelling. International Society for Magnetic Resonance in Medicine: Twelfth Scientific Meeting and Exhibition. 2004 May 15-21;(1360)

[8] Haacke, Brown, Thompson and Venkatesan (1999) Magnetic Resonance Imaging: Physical Principles and Sequence Design (Chapt. 1-4, 20-22, 27), Wiley-Liss.

[9] Hoge RD, Atkinson J, Gill B, Crelier GR, Marrett S, Pike GB.Investigation of BOLD signal dependence on cerebral blood flow and oxygen consumption: the deoxyhemoglobin dilution model. Magn Reson Med. 1999 Nov;42(5):849-63.

[10] Kimmich R. NMR Tomography Diffusometry Relaxometry. Springer-Verlag, Berlin. 1997.

[11] Luh WM, Wong EC, Bandettini PA, Hyde JS. QUIPSS II with thin-slice TI1 periodic saturation: a method for improving accuracy of quantitative perfusion imaging using pulsed arterial spin labeling.Magn Reson Med. 1999 Jun;41(6):1246-54.

[12] Maccotta L, Detre J, Alsop D. The Efficiency of Adiabatic Inversion for Perfusion Imaging by Arterial Spin Labeling. NMR in Biomedicine. 1997 Jun-Aug;10(4-5): 216-221.

[13] Mani S, Pauly J, Conolly S, Meyer C, Nishimura D. Background Suppression with Multiple Inversion Recovery Nulling: Applications to Projective Angiography. Magn Reson Med. 1997 Jun;37(6): 898-905.

[14] R.J. Ordidge, M. Wylezinska, J.W. Hugg, E. Biutterworth and F. Franconi , Frequency offset corrected inversion (FOCI) pulses for use in localized spectroscopy. Magn Reson Med 36 (1996), pp. 562-566.

[15] G.S. Payne and M.O. Leach In: Implementation and evaluation of frequency offset corrected inversion (FOCI) pulses on a clinical MR system 38 (1997), pp. 828-833.

[16] Rosenfeld D, Panfil SL, Zur Y. Design of adiabatic pulses for fat-suppression using analytic solutions of the Bloch equation.Magn Reson Med. 1997 May;37(5):793-801.

[17] Santyr GE. Magnetization transfer effects in multislice MR imaging. Magn Reson Imaging. 1993;11(4):521-32. Erratum in: Magn Reson Imaging 1993;11(7):1083.

[18] Smith, Mari A., Hu Haitao, Shaka A. J. , Improved Broadband Inversion Performance for NMR in Liquids. Journal of Magnetic Resonance 151 (2001), pp. 269-283.

[19] M.S. Silver, R.I. Joseph and D.I. Hoult , Selective Spin Inversion in Nuclear Magnetic Resonance and Coherent Optics Through an Exact Solution of the Bloch-Ricatti Equation. J Magn Reson 31 (1985), pp. 2753-2755.

[20] Tannus A, Garwood M.Adiabatic pulses. NMR Biomed. 1997 Dec;10(8):423-34. Review.

[21] Williams DS, Detre JA, Leigh JS, Koretsky AP. Magnetic resonance imaging of perfusion using spin inversion of arterial water.Proc Natl Acad Sci U S A. 1992 Jan 1;89(1):212-6. Erratum in: Proc Natl Acad Sci U S A 1992 May 1;89(9):4220.

[22] Ye FQ, Frank JA, Weinberger DR, McLaughlin AC. Noise Reduction in 3D Perfusion Imaging by Attenuating the Static Signal in Arterial spin Tagging (ASSIST). Magn Reson Med. 2000 July; 44(1): 92-100.

[23] M.N. Yongbi, Y. Yang, J.A. Frank and J.H. Duyn , Multislice perfusion imaging in human brain using the C-FOCI inversion pulse: comparison with hyperbolic secant. Magn Reson Med 42 (1999), pp. 1098-1105.